Work/Energy Analysis of Bending Limit Cycles in a Deadband Attitude Control System

Franklin C. Loesch* and Calvin Hecht†
The Aerospace Corp., El Segundo, Calif.

An analysis of the interactions between a nonlinear attitude control system and a flexible spacecraft is performed by applying work/energy and impulse/momentum principles. The control elements include a rate gyro; electronic components for integration, summing, filtering and switching; and a pair of opposing gas thrusters controlled by solenoid valves. The analysis accounts for the nonlinear characteristics of the switching elements and the thruster time delays. The thruster time delay has a primary effect in limiting the growth of transient oscillations and is a significant parameter in determining types of limit cycles. The objectives of the analysis are to predict transient bending oscillation growth rates, bending limit cycle frequencies, amplitudes, average attitude angles, and thruster firing ratios. Simple formulas are developed which predict the characteristics of the stable limit cycles and a growth limiting boundary. Digital simulation results verify the accuracy of these predictions. The work/energy approach and the simple, accurate prediction of limit cycle characteristics and boundaries are novel features of the analysis.

Introduction

THE use of a relay control system on a flexible spacecraft is an example of a system in which limit cycles occur due to the nonlinearities of the control system. In this paper, work/energy methods are used to analyze the characteristics of these limit cycles. The first part of the paper describes the problem and develops analytic results for steady-state behavior. Later, the work/energy results are used to analyze transient behavior and to develop criteria for restricting the amplitude of the limit cycles.

The attitude control system considered here has two nonlinear features of primary interest: 1) switching elements, and 2) solenoid valves and thrusters. These two nonlinear features are characterized quantitatively by the discontinuity and equivalent deadband pull-in rate of the switch, and by the nonlinear time delay associated with the solenoid valve and thrusters. The pull-in rate is defined as the magnitude of the error signal at which the switch applies voltage to either solenoid valve. The solenoid-thruster ON and OFF time delay is the time elapsed between command application to, or removal from, the solenoid, and the beginning or removal of thrust application. Because removal of the input command before the time delay has elapsed inhibits thrust, this second nonlinear feature cannot be modeled by the conventional transport lag equation.

The technologies involved in the treatment of systems of the type of which this paper is concerned include stability and control of nonlinear systems, control of flexible vehicles, and work/energy methods. Regarding the stability of nonlinear control systems, a vast amount of literature has been published which describes mathematical methods for analyzing stability of nonlinear control systems based on application of Liapunov's (Lyapunov, Liapounov) second (direct) method.[1] References (1-3) are texts which give the theory and application of Liapunov's method for determining stability, and contain historical information related to this subject. Liapunov techniques are generally concerned with asymptotic stability and require, as a criterion for stability, the evaluation of a certain Eulerian derivative. Although these requirements prohibit direct use of the method for relay control systems, work has been done on constructing Liapunov functions by compter techniques[4] that can be applied to these systems. Liapunov methods applied to system design, including continuous and discrete time systems, are described in Ref. 5. A survey paper[6] in 1966 on the status of stability theory for nonlinear systems contained a section on aerospace application, but made no reference to relay control systems.

Control of flexible spacecraft has been a topic of concern since the middle 1950's. References 7 and 8 are recent papers giving comprehensive treatments of analysis methods and stability determination for control systems on flexible vehicles. While comprehensive, these treatments require extension in order to cover the type of control system nonlinearities treated herein.

Energy methods were used successfully in some of the earlier work on spinning space vehicles. In Refs. 9 and 10, the structural damping dissipation work due to the flexibility of the spinning vehicle is used to determine the rate of decrease of kinetic energy and the consequent change in orientation of the spin axis. The present paper extends the work/energy principles used in 9 and 10 to include work done on the spacecraft by an active, nonlinear control system.

The conventional analytical method for treating systems with the switching type of nonlinearity of this paper is the describing-function analysis, Refs. 2, 3, and 11. The describing-function analysis of a nonlinear system is based on three assumptions[11]: 1) there is only one nonlinear element in the system, or if there is more than one, all nonlinearities are considered as a single nonlinear component; 2) No time varying characteristics are included in the nonlinear element; and 3) if the input is a sinusoidal signal, only the fundamental component of the output of the nonlinear element contributes to the input. The sinusoidal response characteristics of the nonlinear element are then expressed in terms of a describing-function, which is defined as the ratio of the fundamental component of the output to the amplitude of the input. In general, the describing-function is a function of both the input amplitude and frequency. After determination of the describing-function's variation with amplitude and frequency of the input signal, one treats the nonlinear element as a component in a linear system except that subsequent analysis must include the dependence of the system response on input signal

Received Aug. 25, 1975; revision received Jan. 26, 1976. This work was supported by the Space and Missile Systems Organization of the Air Force Systems Command under Contract F04701-74-6-0075. We gratefully acknowledge the support of the Project Officer, Lt. Col. A.H. Dietz.

Index categories: Spacecraft Attitude Dynamics and Control; LV/M Dynamics and Control.

*Head of Program Management Support, Reentry Systems Division.

†Member of the Technical Staff, Guidance and Control Division.

level. All of the usual linear frequency-response methods can be applied to determine system stability, conditions under which sustained oscillations exist, and evaluation of system performance with sinusoidal input functions.

The work/energy analysis methods developed in this paper require assumptions (2) and (3) above, but are not restricted to a single nonliner element. Work/energy methods not only determine conditions under which sustained oscillations can occur, as in the describing-function method, but also determine the characteristics of these oscillations. As demonstrated in Fig. 5, work/energy methods accurately predict the type of limit-cycles which occur, single or double-sided pulsing, and the frequency ratio of torquing pulses as a function of input constant torque. The basic describing-function analysis technique would need modification to evaluate systems with a constant input, and could not give the results depicted in Fig. 5. Among other basic differences between describing-function and the work/energy analysis methods developed in this paper, one notes that because the frequency-response methods used with the describing-function are basically steady-state techniques, they cannot produce the transient analysis results obtained in the later sections of this paper.

Transient bending oscillations at the natural frequency of the spacecraft are caused by disturbance torques or the application or removal of control thrust for commanded maneuvers. In Ref. 12, and in this paper, it is shown how these transient oscillations may grow as the result of cyclic thruster activity to become limit cycles. The first results developed are based on the assumption that steady-state limit cycle conditions have been achieved. The ability to predict the characteristics of these limit cycles is important to control system designers in order to insure that attitude control accuracy requirements are met. The essential parameters of the bending limit cycle are the frequency, the bending amplitude, the firing ratio of each thruster, and the average attitude angle. All four of these limit cycle parameters are predicted by analytic formulas derived by applying work/energy, impulse/momentum, and force/equilibrium laws.

The later results developed in this paper include an analytic criterion which determines whether the system can or cannot reach a double-firing limit cycle. The accuracy of this criterion is verified by computer simulations of the system analyzed. A criterion for the prevention of double-firing limit cycles is important in order that large bending amplitudes and high rates of gas consumption may be avoided.

Description of Control System

The pitch channel of the idealized attitude control system, which is analyzed by work/energy methods, is shown in Fig. 1. As indicated by the transfer function in the rate gyro block of Fig. 1, the rate gyro's gain and phase lag are given by

$$\text{Gain} = \frac{|\text{Output}|}{|\text{Input}|} = \frac{1}{\left\{\left[1-\left(\frac{\omega_1}{\omega_{ng}}\right)^2\right]^2 + \left[2\zeta_g \frac{\omega_1}{\omega_{ng}}\right]^2\right\}^{1/2}} \tag{1a}$$

$$\tan\phi = [2\zeta_g(\omega_1/\omega_{ng})]\,[1-(\omega_1/\omega_{ng})^2]^{-1} \tag{1b}$$

In Eq. (1) ϕ = phase lag of rate gyro, ζ_g = damping coefficient of rate gyro, ω_{ng} = undamped natural frequency of rate gyro, and ω_1 = frequency of sinusoidal input rate.

The rate gyro signal, $\dot{\theta}$, is integrated. In this description it is assumed that the commanded attitude is zero. The rate and integrated rate are summed to provide an error signal entering a first-order filter of:

$$\text{Filter Input} = \dot{\theta} + \theta/\lambda; \text{ where } 1/\lambda = \text{attitude gain} \tag{2}$$

As indicated by the filter block in Fig. 1, the first-order filter frequency response is given by

$$\left.\begin{aligned}\text{Gain} \equiv \frac{|\text{Output}|}{|\text{Input}|} &= \frac{1}{[1+(\omega_1 t_2)^2]^{1/2}} \\ \text{Phase Lag} &= \tan^{-1}(\omega_1 t_2)\end{aligned}\right\} \text{where } t_2 = \text{filter time constant} \tag{3}$$

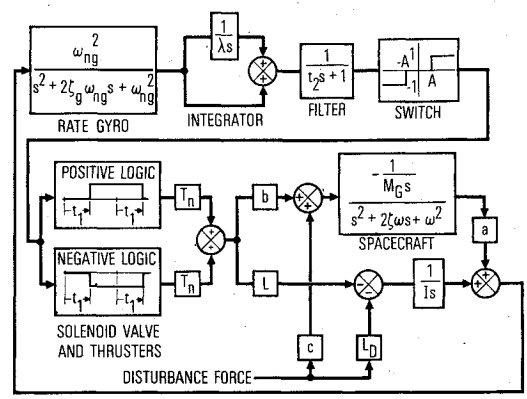

Fig. 1 Block diagram of idealized control system and digital simulation.

Let E represent the filter output. The switch controls the voltage to the thruster solenoid values according to the following rules

Negative Pitch Nozzle	Positive Pitch Nozzle
Voltage ON if: $E \geq A$	Voltage ON if: $E \leq -A$
Voltage OFF if: $E < A$	Voltage OFF if: $E > -A$

(4)

where A is the amplitude of the pull-in rate. We neglect the hysteresis of the switch which causes voltage OFF to occur at a magnitude of E slightly less than the magnitude of A. Although including nonzero hysteresis in our analysis is not fundamentally difficult, it complicates the formulations to achieve only negligible improvements in accuracy.

The solenoid values and nozzles are idealized by assuming that thrust is a constant and that full thrust comes on instantaneously, t_1 sec after the voltage ON command is received from the switch. Correspondingly, thrust falls instantaneously to zero, t_1 sec after the voltage OFF command is received. If voltage OFF occurs before t_1 has elapsed from a prior voltage ON command, no thrust pulse occurs, and if voltage ON occurs before t_1 has elapsed from a prior voltage OFF command, thrust stays ON continuously.

Spacecraft Dynamics

The spacecraft on which the control system is mounted is flexible in bending and has a series of natural frequencies and corresponding mode shapes. Our analysis assumes that the oscillation frequency is very nearly equal to the first natural bending frequency of the system; therefore, the oscillation shape is very nearly the corresponding first natural mode shape. Consideration of the first mode only is a good approximation because the rate gyro natural frequency and filter time constant will normally be selected so that the higher modes' amplitudes are greatly attenuated. The analysis also assumes that the disturbance torque is constant.

Figure 2 shows schematically the assumed spacecraft dynamic system. Let dm/dx be the mass per unit length of the spacecraft, and let di/dx be the moment of inertia per unit length. The kinetic energy of the spacecraft is

$$KE = \frac{1}{2}\int_{-x_1}^{x_2} (\dot{y}_{cm} + x\dot{\theta}_{\text{avg}} + \dot{y}(x,t))^2 \left(\frac{dm}{dx}\right) dx + \frac{1}{2}\int_{-x_1}^{x_2} (\dot{\theta}_{\text{avg}} + \dot{\theta}(x,t))^2 \left(\frac{di}{dx}\right) dx \tag{5}$$

We assume that the spacecraft bending oscillation is a pure natural modal oscillation. This assumption implies that $\dot{y}$ and $\dot{\theta}$ in Eq. (5) are given by

$$\dot{y}(x,t) = \left(\frac{\dot{y}(x)}{\dot{y}_0}\right)\dot{y}_0 \sin\omega t; \quad \dot{\theta}(x,t) = \left(\frac{\dot{\theta}(x)}{\dot{y}_0}\right)\dot{y}_0 \sin\omega t \tag{6}$$

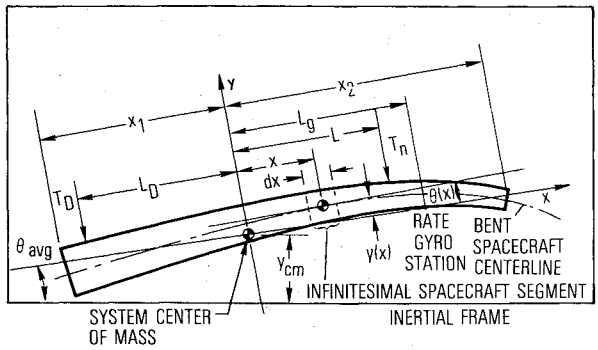

Fig. 2 Schematic of spacecraft dynamics. L = distance from system center of mass to control thruster; L_D = distance from system center of mass to disturbance force; L_g = distance from system center of mass to rate gyro; T_D = disturbance force; T_n = control nozzle thrust (shown for nozzle #1, nozzle #2 thrust is in opposite sense); $y(x)$ = deflection of infinitesimal segment in y direction; y_{cm} = deflection of center of mass in y direction; $\theta(x)$ = angular deflection of deformed spacecraft centerline at location x, measured from undeformed centerline; and θ_{avg} = angular deflection of undeformed spacecraft centerline.

where

ω = modal natural frequency (7a)

$\dot{y}_0$ = velocity amplitude at an arbitrarily selected normalizing station, x_0 (7b)

$\dot{y}(x)/\dot{y}_0$ = normalized modal deflection amplitude function (7c)

$\dot{\theta}(x)/\dot{y}_0$ = normalized modal slope amplitude function (7d)

Substituting this assumed modal oscillation into Eq. (5) and imposing the requirements for a natural modal oscillation that the rate of change with time of the net lateral momentum and the net moment of lateral momentum must be zero, Eq. (5) for the kinetic energy simplifies to

$$KE = \tfrac{1}{2}M\dot{y}_{cm}^2 + \tfrac{1}{2}I\dot{\theta}_{avg}^2 + \tfrac{1}{2}M_G\dot{y}_0^2\sin^2\omega t \tag{8}$$

In Eq. (8) M = total mass, I = total moment of inertia about the system center of mass and

$$M_G \equiv \int_{-x_1}^{x_2}\left[\left(\frac{\dot{y}(x)}{\dot{y}_0}\right)^2\frac{dm}{dx} + \left(\frac{\dot{\theta}(x)}{\dot{y}_0}\right)^2\frac{di}{dx}\right]dx$$

= generalized mass (9)

M_G is a constant determined by the normalized mode shape of the spacecraft and the spacecraft inertial properties. Since $\dot{y}_0$ is the rate deflection amplitude at an arbitrary normalizing station, x_0, the generalized mass of the normal mode will vary for different choices of x_0. One popular method is to choose x_0 so that M_G = M, but any normalizing station may be used.

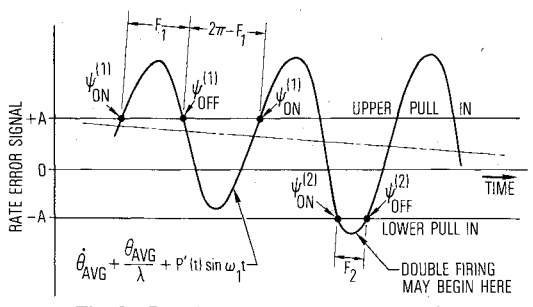

Fig. 3 Bending oscillation characteristics.

The maximum value of kinetic energy represents the total energy of the system, since strain and kinetic energy are interchanged cyclically in the modal oscillation. The maximum kinetic energy is given by Eq. (8) with $\sin\omega t = 1$.

Conservation of momentum requires that the rate of change of $\dot{y}_{cm}$ and $\dot{\theta}_{avg}$ be determined by the external forces acting on the spacecraft, namely the nozzle thrust T_n and the disturbance force T_D. Applying Lagrange's equations of motion to Eq. (8) and integrating over a time interval consisting of N complete cycles of period $(2\pi/\omega_1)$, we obtain the following impulse/momentum relations (let $\omega_1 t = \psi$)

$$M\Delta\dot{y}_{cm} = M\int_{\dot{y}_{cm}}^{\dot{y}_{cm}+\Delta\dot{y}_{cm}} d(\dot{y}_{cm}) = -\int_0^{N(2\pi/\omega_1)}(T_n + T_D)\,dt$$

$$= -1/\omega_1\int_0^{2\pi N}(T_n + T_D)\,d\psi \tag{10a}$$

$$I\Delta\dot{\theta}_{avg} = I\int_{\dot{\theta}_{avg}}^{\dot{\theta}_{avg}+\Delta\dot{\theta}_{avg}} d(\dot{\theta}_{avg}) = \int_0^{N(2\pi/\omega_1)}(-T_nL + T_DL_D)\,dt$$

$$= 1/\omega_1\int_0^{2\pi N}(-T_nL + T_DL_D)\,d\psi \tag{10b}$$

Referring to Fig. 2, let the amplitude of $\dot{\theta}$ at station $x = L_g$ be denoted by P. Define the following amplitude influence coefficients of the natural mode shape as defined by Eq. (6)

$$a \equiv \dot{\theta}(L_g)/\dot{y}_0 \equiv P/\dot{y}_0 \quad b \equiv \dot{y}(L)/\dot{y}_0 \quad c \equiv \dot{y}(L_D)/\dot{y}_0 \tag{11}$$

Over a time interval of N cycles, let ΔKE_{max}, $\Delta\dot{y}_{cm}$, $\Delta\dot{\theta}_{avg}$, and ΔP be the respective changes in these quantities, and define the average values during this interval as $\overline{\dot{y}_{cm}} = \dot{y}_{cm} + (\tfrac{1}{2})\Delta\dot{y}_{cm}$; $\overline{\dot{\theta}_{avg}} = \dot{\theta}_{avg} + (\tfrac{1}{2})\Delta\dot{\theta}_{avg}$; $\bar{P} = P + (\tfrac{1}{2})\,\Delta P$; then using Eq.(11) and Eq. (8) with $\sin\omega t = 1$, ΔKE_{max} is given by

$$\Delta KE_{max} = M\overline{\dot{y}_{cm}}\Delta\dot{y}_{cm} + I\overline{\dot{\theta}_{avg}}\Delta\dot{\theta}_{avg} + (M_G/a^2)\,\bar{P}\Delta P \tag{12}$$

By substituting for $\Delta\dot{y}_{cm}$ and $\Delta\dot{\theta}_{avg}$ using Eq. (10) and remembering that we assume a constant disturbance force, this expression for ΔKE_{max} becomes

$$\Delta KE_{max} = T_D\left(\frac{2\pi N}{\omega_1}\right)\left(-\overline{\dot{y}_{cm}} + L_D\overline{\dot{\theta}_{avg}}\right)$$

$$-\frac{1}{\omega_1}\left(\overline{\dot{y}_{cm}} + L\overline{\dot{\theta}_{avg}}\right)\int_0^{2\pi N}T_n\,d\psi + \frac{M_G}{a^2}\,\bar{P}\Delta P \tag{13}$$

Switching and Nozzle Phasing

In addition to the assumptions defined above, our analysis of bending limit cycles makes three additional basic assumptions: a) the oscillatory portion of the error signal is very nearly a pure sine wave at the switch input; b) the attitude gain and frequency have values such that $(1/\lambda\omega_1) << 1$; and c) the changes in the bending rate amplitude, the average attitude, the average attitude rate, and the lateral center of mass velocity in one bending cycle are each small compared to the average value of the respective quantity during the cycle.

The assumed motion shown in Fig. 3 consists of slowly varying y_{cm} and θ_{avg} motions superposed on the natural modal oscillation at frequency ω_1. Due to a combination of the structural bending at frequency ω_1 with rate amplitude P plus the average θ and $\dot{\theta}$ motions, the #1 nozzle is firing ON and OFF. As indicated in Fig. 3, nozzle #2 may or may not be firing, but in order to derive the equations in their most general form, we assume initially that nozzle #2 is firing. Referring to Figs. 2 and 3, it is seen that at the rate gyro location the assumed motion is

$$\theta = \theta_{avg} - (P/\omega_1)\cos\omega_1 t \tag{14a}$$

$$\dot{\theta} = \dot{\theta}_{avg} + P[\sin\omega_1 t - (\dot{P}/P\omega_1)\cos\omega_1 t] \tag{14b}$$

The bending rate amplitude P is modified by the combined gains of the rate gyro and filter so that the rate amplitude is changed to P' at the switch input. Using Eqs. (1) and (3), we define the combined gain factor, G, which relates P' to P, thus

$$\frac{P'}{P}=\left(\frac{1}{[1+(\omega_l t_2)^2]^{1/2}}\right)$$

$$\times\left(\frac{1}{\left\{\left[1-\left(\frac{\omega_l}{\omega_{ng}}\right)^2\right]^2+\left[2\zeta_g\frac{\omega_l}{\omega_{ng}}\right]^2\right\}^{1/2}}\right)\equiv G \qquad (15)$$

Using Eq. (2), it is seen that the exact pull-in condition for the switch which corresponds to the assumed motion of Eq. (14) is

$$\dot\theta+\theta/\lambda=\dot\theta_{avg}+\theta_{avg}/\lambda+P'[\sin\omega_l t-(\dot P'/P'\,\omega_l)\cos\omega_l t]$$
$$-(P'/\omega_l\lambda)\cos\omega_l t=\pm A \qquad (16)$$

We neglect the $P'/(\lambda\omega_l)$ term, compared to the P' term, in accord with assumption (b) mentioned previously. We neglect also the $\dot P'/(P'\omega_l)$ term, relative to one, in accord with assumption (c). Using these approximations, the pull-in condition is

$$\dot\theta_{avg}+\theta_{avg}/\lambda+P'\sin\omega_l t\cong\pm A \qquad (17a)$$

or, solving for $\omega_l t$

$$\omega_l t=\psi=\sin^{-1}\left[\pm\frac{A}{P'}-\frac{E_{avg}}{P'}\right];\ E_{avg}=\dot\theta_{avg}+\frac{\theta_{avg}}{\lambda} \qquad (17b)$$

Thus, referring to Fig. 3, it is seen that, for a system with no phase lags in filter or gyro, the voltage ON and OFF commands for nozzles #1 and #2 would occur at the following angular positions ($\psi=\omega_l t$)

$$\psi_{ON}^{(1)}=\pi/2-F_1/2;\ \psi_{OFF}^{(1)}=\pi/2+F_1/2;\ \psi_{OFF}^{(1)}-\psi_{ON}^{(1)}=F_1 \qquad (18a)$$

$$\psi_{ON}^{(2)}=3\pi/2-F_2/2;\ \psi_{OFF}^{(2)}=3\pi/2+F_2/2;\ \psi_{OFF}^{(2)}-\psi_{ON}^{(2)}=F_2 \qquad (18b)$$

and, in the light of Eq. (17), the angles F_1 and F_2 are evidently

$$F_1=\pi-2\sin^{-1}\left[\frac{1-(E_{avg}/A)}{P'/A}\right]$$

$$F_2=\pi-2\sin^{-1}\left[\frac{1+(E_{avg}/A)}{P'/A}\right] \qquad (19)$$

In Eq. (19), the sign of the argument of the inverse sine in the F_2 equation has been reversed and both inverse sines are defined to lie between $-\pi/2$ and $+\pi/2$. This definition makes Eqs. (18) and (19) compatible. In the real system, the voltage ON or OFF command to the nozzle solenoid is delayed by the sum of the filter and the rate gyro phase lag. After voltage is applied to or removed from the solenoid, a time delay, t_l, occurs before the thrust comes ON or turns OFF. Thus, in order to obtain the angular position at which thrust actually comes ON or goes OFF, we must add to all four of the ON and OFF commands of Eq. (18) an angular delay, or phase shift, of

$$\Delta\psi=\tan^{-1}\omega_l t_2+\phi+\omega_l t_l \qquad (20)$$

In accord with our assumptions of solenoid valve behavior, we note by referring to Fig. 3 that

Nozzle #1 will turn ON only if: $\omega_l t_l<F_1$ (21a)

Nozzle #1 will turn OFF only if: $\omega_l t_l<(2\pi-F_1)$ (21b)

Nozzle #2 will turn ON only if: $\omega_l t_l<F_2$ (21c)

Work/Energy and Impulse/Momentum Requirements

Refer to Fig. 2. The elemental work done on the spacecraft by the negative nozzle (nozzle #1) is

$$dW=-T_n[\dot y_{cm}+L\dot\theta_{avg}+\dot y(L)\sin\omega_l t]\,dt \qquad (22)$$

in which $\dot y(L)$ = bending deflection velocity amplitude at nozzle location, L, and $\dot y(L)=Pb/a$, $(a\neq 0)$, in accord with the definitions of Eq. (11). Thus, Eq. (22) becomes

$$dW=-T_n\left(\dot y_{cm}+L\dot\theta_{avg}+\frac{b}{a}P\sin\omega_l t\right)dt;\ \text{nozzle \#1} \qquad (23)$$

The work done by nozzle #2 is given by the above expression with reversed sign. Using Eq. (11), the elemental work done by the constant disturbance force is

$$dW=-T_D\left[\dot y_{cm}-L_D\dot\theta_{avg}+\frac{c}{a}P\sin\omega_l t\right]dt \qquad (24)$$

The generalized structural damping dissipation force is $2\zeta\omega M_G\dot y_0\sin\omega_l t$, where ζ is the structural damping coefficient and ω_l is the oscillation frequency which may be slightly different than ω, the natural modal frequency. The

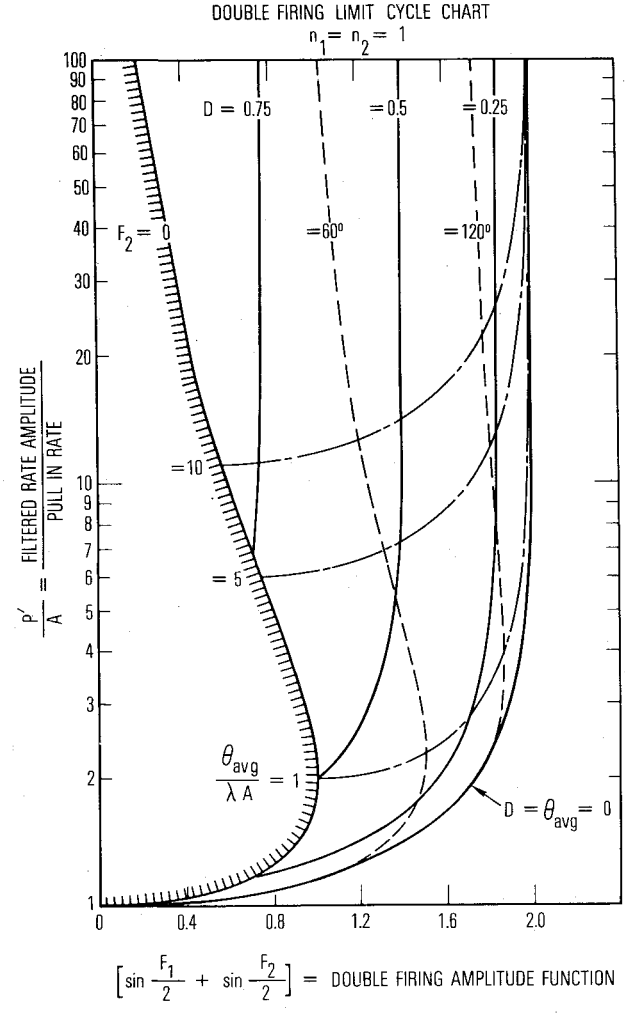

Fig. 4 Double-firing limit cycle chart.

dissipative work done by this force in time dt is, using Eq. (11)

$$dW = (-2\zeta\omega M_G \dot{y}_0 \sin\omega_1 t)\dot{y}_0 \sin\omega_1 t\, dt$$

$$= -2\zeta\omega M_G (P/a)^2 \sin^2\omega_1 t\, dt \tag{25}$$

Let N be an integral number of cycles of oscillation. Let N_1 be the number of nozzle #1 ON-OFF pulses which occur during N cycles; and let N_2 be the number of nozzle #2 ON-OFF pulses which occur. It is assumed that neither nozzle's thrust pulses are bunched but are approximately uniformly distributed over the N cycles. Integrate each of Eqs. (23-25) over N cycles and sum the results in order to obtain the work done on the spacecraft by the nozzles, the disturbance force, and the structural damping. Equate this resulting total work input over N cycles to the increase in spacecraft maximum kinetic energy in N cycles as given by Eq. (13). Use Eqs. (18) and (20) to specify the limits of integration for those integrals which involve the nozzle thrust. In carrying out the integrations, assume that the quantities $\dot{y}_{cm}$, $\dot{\theta}_{avg}$, θ_{avg}, and P vary slowly enough so that over one cycle of oscillation each quantity may be considered approximately constant, and may be taken outside the respective integration. Let the subscript i indicate the value of each quantity during the i^{th} cycle. By these steps and assumptions we obtain the following work/energy equation

$$\frac{T_n}{\omega_1}\left[-\frac{N_1}{N}\sum_{i=1}^{N}(\dot{y}_{cm}+L\dot{\theta}_{avg})_i\int_{\pi/2-(F_1/2)_i+\Delta\psi}^{\pi/2+(F_1/2)_i+\Delta\psi}d\psi+\frac{N_2}{N}\sum_{i=1}^{N}(\dot{y}_{cm}+L\dot{\theta}_{avg})_i\int_{3\pi/2-(F_2/2)_i+\Delta\psi}^{3\pi/2+(F_2/2)_i+\Delta\psi}d\psi\right]$$

$$+\frac{T_n b}{a\omega_1}\left[-\frac{N_1}{N}\sum_{i=1}^{N}\tilde{P}_i\int_{\pi/2-(F_1/2)_i+\Delta\psi}^{\pi/2+(F_1/2)_i+\Delta\psi}\sin\psi d\psi+\frac{N_2}{N}\sum_{i=1}^{N}P_i\int_{3\pi/2-(F_2/2)_i+\Delta\psi}^{3\pi/2+(F_2/2)_i+\Delta\psi}\sin\psi d\psi\right]$$

$$-\frac{T_D}{\omega_1}\left[\sum_{i=1}^{N}(\dot{y}_{cm}-L_D\dot{\theta}_{avg})_i\int_0^{2\pi}d\psi+\frac{c}{a}\sum_{i=1}^{N}P_i\int_0^{2\pi}\sin\psi d\psi\right]$$

$$-2\zeta\left(\frac{\omega}{\omega_1}\right)\left(\frac{M_G}{a^2}\right)\sum_{i=1}^{N}P_i^2\int_0^{2\pi}\sin^2\psi d\psi = T_D\frac{2\pi N}{\omega_1}(-\overline{\dot{y}_{cm}}+L_D\overline{\dot{\theta}_{avg}})+\frac{M_G}{a^2}\tilde{P}\Delta P$$

$$+\frac{T_n}{\omega_1}(\overline{\dot{y}_{cm}}+L\overline{\dot{\theta}_{avg}})\left[-\frac{N_1}{N}\sum_{i=1}^{N}\int_{\pi/2-(F_1/2)_i+\Delta\psi}^{\pi/2+(F_1/2)_i+\Delta\psi}d\psi+\frac{N_2}{N}\sum_{i=1}^{N}\int_{3\pi/2-(F_2/2)_i+\Delta\psi}^{3\pi/2+(F_2/2)_i+\Delta\psi}d\psi\right] \tag{26}$$

Steady-State Limit Cycles

We assume that over a large number of cycles a steady-state limit cycle exists; i.e., that P and θ_{avg} are constant. With constant P and θ_{avg}, it follows that F_1 and F_2 are constant and that $\dot{\theta}_{avg}$ is zero. By imposing this steady-state assumption on Eq. (26), carrying out the integrations and simplifying we obtain

$$\left[\frac{T_n}{\omega_1}(-N_1F_1+N_2F_2)-\frac{2\pi NT_D}{\omega_1}\right]\left[\left(\frac{1}{N}\sum_{i=1}^{N}(\dot{y}_{cm})_i\right)-(\overline{\dot{y}_{cm}})\right]$$

$$-\frac{2T_n bP}{a\omega_1}\left[N_1\sin\frac{F_1}{2}+N_2\sin\frac{F_2}{2}\right]\cos\Delta\psi$$

$$-N\left[2\pi\zeta\left(\frac{\omega}{\omega_1}\right)M_G\left(\frac{P}{a}\right)^2\right]=0 \tag{27}$$

Since in the steady-state $\dot{y}_{cm}$ changes by the same amount on each cycle, it follows that the second bracket in the first term is zero; hence, after dropping the first term and rearranging, Eq. (27) becomes

$$\frac{P}{A} = -Q\left[n_1\sin\frac{F_1}{2}+n_2\sin\frac{F_2}{2}\right]\cos\Delta\psi \tag{28}$$

in which we have defined n_1 = nozzle #1 firing ratio $= N_1/N$, n_2 = nozzle #2 firing ratio $= N_2/N$ and

$$Q \equiv \text{nondimensional torque parameter} \equiv \frac{T_n ab}{\pi\zeta M_G\omega A} \tag{29}$$

Under the steady-state assumption that $\dot{\theta}_{avg}$ and $\Delta\dot{\theta}_{avg}$ are zero, the angular impulse requirement of Eq. (10) applied over N cycles gives, with $D = (T_D L_D)/(T_n L) =$ disturbance to control torque ratio

$$n_1F_1 - n_2F_2 = 2\pi D \tag{30a}$$

However, for the case in which nozzle #2 is not firing, i.e., $n_2 = 0$, and in which $n_1 < 1$, but the nozzle #1 ON pulse duration is greater than one full cycle, the angular impulse/momentum law must be changed to

$$2\pi - n_1(2\pi - F_1) = 2\pi D \tag{30b}$$

Equations (28), (30a) and (30b), together with the restrictions of relation (21), provide the three basic equations from which we can determine limit cycle amplitudes, firing ratios, and average attitude angle.

Permissible Frequency Ranges

Real limit cycles can exist only if the amplitude, P, given by Eq. (28) is positive. Physically, in order to have a positive solution for the amplitude P from Eq. (28), the nozzle work input must be positive; otherwise, the steady-state cycle cannot be maintained. The quantities ζ, M_G, ω, ω_1, n_1 and n_2 are all positive inherently, and A and T_n are positive by definition. Since neither F_1 nor F_2 can exceed 2π, then $\sin F_1/2$ and $\sin F_2/2$ must always be positive; hence positive solutions for P exist only if

$$-ab\cos\Delta\psi > 0 \tag{31}$$

For given values of rate gyro damping and natural frequency, filter time constant, and nozzle time delay, this inequality determines a range of bending frequencies within which bending limit cycles may occur, but outside of which they cannot occur. For example, if $ab > 0$, steady-state bending limit cycles can occur only for bending frequencies which result in negative $\cos\Delta\psi$ or for $\Delta\psi$ in the range: $(\pi/2) < \Delta\psi < (3\pi/2)$.

Double-Firing Limit Cycles

Consider first the case where both nozzles fire on every cycle so that $n_1 = n_2 = 1$. Equation (30a) simplifies to

$$F_1 - F_2 = 2\pi D \tag{32}$$

and using the definitions of F_1 and F_2 in Eq. (19), this may be rearranged as follows after taking the cosine of both sides,

squaring, and simplifying

$$\frac{\theta_{avg}}{\lambda A} = \left[\left(\frac{P'}{A}\right)^2 \sin^2\left(\frac{\pi}{2}D\right) - \tan^2\left(\frac{\pi}{2}D\right)\right]^{1/2} \qquad (33)$$

Combining Eqs. (15) and (28) for this case gives

$$\frac{P'}{A} = -GQ\cos\Delta\psi\left[\sin\frac{F_1}{2} + \sin\frac{F_2}{2}\right] \qquad (34)$$

Eqs. (33) and (34) determine implicitly P'/A and $\theta_{avg}/(\lambda A)$ for given values of D, Q, G, and $\Delta\psi$. A trial process may be used to solve for P'/A and $\theta_{avg}/(\lambda A)$; then P/A is determined by Eq. (15).

Figure 4 shows P'/A plotted vs the double-firing amplitude function, $\sin(F_1/2)+\sin(F_2/2)$, for assigned values of D. Also shown on Fig. 4 are lines of F_2 and $\theta_{avg}/(\lambda A)$. It is clear that unless the solenoid time delay is small, inequality (21) will be violated as the disturbance torque increases. For example, if the phase delay of the solenoid, $\omega_1 t_1$, were 120 deg and P'/A were 8, then $\omega_1 t_1 > F_2$ for all $D > .25$; therefore, nozzle #2, according to inequality (21), will not turn ON, and the assumption that $n_2 = 1$ is clearly invalid for $D > .25$ in this example. If n_2 is allowed to be less than one, however, a quasi-stable operating condition can be established in which, for given P'/A, θ_{avg} is not allowed to increase as the disturbance torque increases. This quasi-stable operating condition is obtained at a value of θ_{avg} which results in the angle F_2 being equal to $\omega_1 t_1$. This operating condition is stable. If n_2, the firing ratio, increases, θ_{avg} increases and F_2 decreases, θ_{avg} will decrease, F_2 increase, and n_2 will increase.

Thus, quasi-steady state, double-firing limit cycles are governed by Eqs. (28) and (30a) with $n_1 = 1$; $0 < n_2 < 1$; and by the condition that

$$F_2 = \omega_1 t_1 \qquad (35)$$

By using Eq. (35) in conjunction with Eqs. (19), (28), and (30a), a series of equations is derived which determiine n_2, P'/A, and $\theta_{avg}/(\lambda A)$ for a given disturbance torque ratio. This set of equations is shown in Table 1 alongside the corresponding equations for steady-state limit cycles. By using the two sets of equations in Table 1, Fig. 5 was computed for the following example values: $Q = 14$; $\omega_1 = 121.8$ sec^{-1}; $\omega_{ng} = 132$ sec^{-1}; $\zeta_g = 0.5$; $t_1 = 0.015$ sec; $t_2 = 0.01$ sec. Figure 5 shows the calculated double-firing amplitude ratio, the nozzle #2 firing ratio, and the average attitude angle ratio as functions of the disturbance torque ratio. Region A is the steady-state region; region B, the quasi-steady-state.

Single-Sided Limit Cycles

If nozzle #2 is not firing at all, bending limit cycles may still occur provided the disturbance torque ratio is neither zero nor

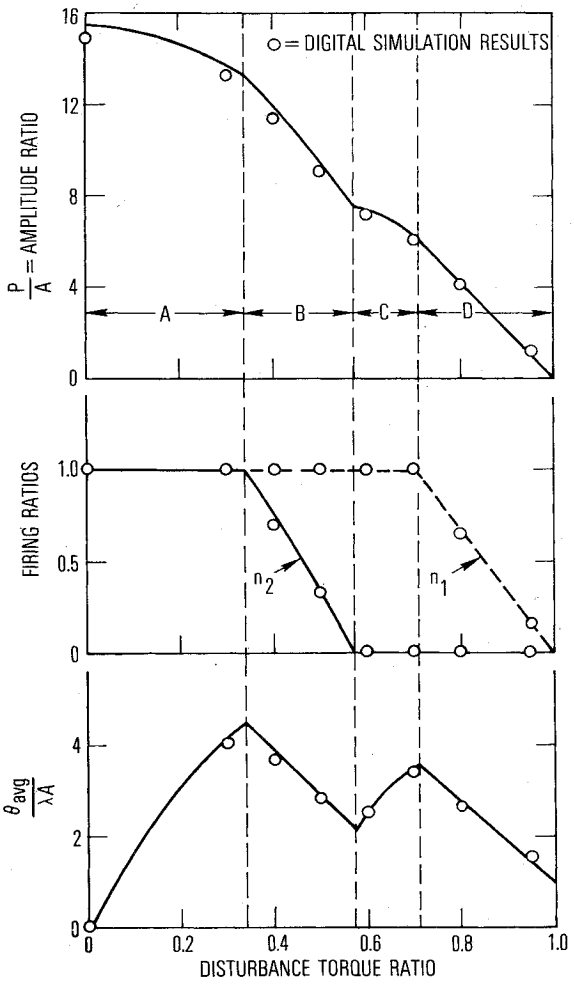

Fig. 5 Bending limit cycles.

one. For these cases $n_2 = 0$. Eqs. (30a) and (30b) become

$$F_1 = 2\pi D/n_1; \text{ or } 2\pi - F_1 = 2\pi(1-D)/n_1 \qquad (36a,b)$$

Substituting the definition of F_1 from Eq. (19), rearranging, and simplifying, we obtain the corresponding relations

$$\theta_{avg}/\lambda A = 1 - (P'/A)\cos(\pi D/n_1);$$

or

$$\theta_{avg}/\lambda A = 1 + (P'/A)\cos[\pi(1-D)/n_1] \qquad (37a,b)$$

Thus, considering inequality (21), it is clear that the firing ratio, n_1, will be one provided that D is not small enough to make F_1 less than $\omega_1 t_1$; also D must not be large enough to

Table 1 Limit cycle formulas[a]

	Double-firing limit cycles		Single-sided limit cycles		
Parameter	Steady-state	Quasi-steady-state	Steady-state	Quasi-steady state	
D	$0 \le D \le D_1$	$D_1 < D \le D_2$	$D > T_1; (1-D) > T_1$	$0 < D \le T_1$	$0 < (1-D) \le T_1$
n_1	1	1	1	D/T_1	$(1-D)/T_1$
n_2	1	$(F_1 - 2\pi D)/\omega_1 t_1$	0	0	0
F_1	Eq. (19)	Eq. (19)	Eq. (19)	$\omega_1 t_1$	$2\pi - \omega_1 t_1$
F_2	Eq. (19)	$\omega_1 t_1$	N/A	N/A	N/A
$\theta_{avg}/\lambda A$	Eq. (33)	$(P'/A)\cos(\pi T_1) - 1$	$1 + \frac{1}{2} q \sin(2\pi D)$	$1 + (n_1/2) q \sin(\omega_1 t_1)$	$1 - (n_1/2) q \sin(\omega_1 t_1)$
P'/A	$-q[\sin(F_1/2) + \sin(F_2/2)]$	$-q[\sin(F_1/2) + n_2 \sin(F_2/2)]$	$G(P/A)$	$G(P/A)$	$G(P/A)$
P/A	$(P'/A)/G$	$(P'/A)/G$	$-Q\cos\Delta\psi\sin(\pi D)$	$-n_1 Q\cos\Delta\psi\sin(\pi T_1)$	$-n_1 Q\cos\Delta\psi\sin(\pi T_1)$

[a] Key:

$T_1 \equiv \omega_1 t_1 / 2\pi$

$q \equiv GQ\cos\Delta\psi$

N/A = not applicable

$$D_1 = \tfrac{1}{2} - T_1 - \frac{1}{\pi}\sin^{-1}\left[\frac{2}{P'/A} - \cos(\pi T_1)\right]$$

$$D_2 = \frac{1}{\pi}\cos^{-1}\left[\frac{2}{P'/A} - \cos(\pi T_1)\right]$$

make $2\pi - F_1$ less than $\omega_1 t_1$. In the steady-state range of D, with $n_1 = 1$, by using Eq. (36a), the amplitude of the limit cycle is given directly by Eq. (28)

$$P/A = -Q\cos\Delta\psi\sin(\pi D); \quad n_1 = 1 \tag{38}$$

In the regions of small or large D, quasi-steady operation is determined by the conditions

$$F_1 = \omega_1 t_1 = 2\pi D/n_1; \quad \text{valid for } 0 < D \leq \omega_1 t_1/2\pi \tag{39a}$$

$$2\pi - F_1 = \omega_1 t_1 = 2\pi(1-D)/n_1;$$

$$\text{valid for } 0 < (1-D) \leq \omega_1 t_1/2\pi \tag{39b}$$

Using Eq. (39) in conjunction with Eqs. (37a, b) and (28), the values of P/A and $\theta_{avg}/(\lambda A)$ are determined for single-sided, quasi-steady-state limit cycles. Results for all three regions are summarized in Table 1. Using the equations in Table 1, the amplitude, firing ratio, and average attitude angle were computed for the same example values listed above. Results are plotted in Fig. 5 as continuations of the double-firing curves. Region C is the steady-state region; region D is the quasi-steady state.

Frequency Shift at Steady-State

For most practical purposes, approximating the steady-state bending limit cycle frequency by the bending natural frequency is adequate. For dynamic equilibrium, however, a small shift of frequency may be required in the steady-state limit cycle so that ω_1, the frequency of the steady-state limit cycle, is slightly different from the bending natural frequency ω. Let the assumed sinusoidal limit cycle bending deflection rate at the nozzle be represented as a vector of amplitude $\dot{y}(L) = \dot{y}_L$ rotating with angular velocity ω_1. The nozzle thrust opposes $\dot{y}_L$ and is required by the control system's characteristics to lag $\dot{y}_L$ by the phase angle $\Delta\psi$. In a rotating vector diagram representing the required force equilibrium for a steady-state limit cycle, the magnitude of the nozzle thrust vector must vary as the vector rotates in such a way as to represent correctly the ON-OFF, constant thrust characteristics of the system; however, the angular position of the nozzle thrust relative to the other vectors which are all rotating at speed ω_1 is fixed by the angle $\Delta\psi$. Since a steady-state sinusoidal oscillation with the first modal bending shape is assumed, the inertial reaction force must lag $\dot{y}_L$ by 90° and be of magnitude $M_G\omega_1\dot{y}_L$. In addition, there must be a structural damping force of $2\zeta M_G\omega\dot{y}_L$ opposing $\dot{y}_L$ and an elastic force of $M_G\omega^2\dot{y}_L/\omega_1$ opposing the inertial reaction. For dynamic equilibrium, we must have the summation of forces perpendicular to and parallel to $\dot{y}_L$ each equal to zero

$$T_n\sin\Delta\psi + M_G\omega^2\frac{y_L}{\omega_1} - M_G\omega_1\dot{y}_L = 0 \tag{40a}$$

$$-T_n\cos\Delta\psi - 2\zeta M_G\omega\dot{y}_L = 0 \tag{40b}$$

By rearranging, dividing, and subsequent rearrangement we obtain:

$$(\omega_1/\omega)^2 + 2\zeta\tan\Delta\psi(\omega_1/\omega) - 1 = 0 \tag{41}$$

For cases of most interest, we may assume $\zeta\tan\Delta\psi << 1$, and the positive root of the quadratic Eq. (41) is closely approximated by:

$$\omega_1/\omega = 1 - \zeta\tan\Delta\psi \tag{42}$$

Thus, the steady-state bending limit cycle frequency is equal to the natural frequency if $\tan\Delta\psi = 0$, or if $\Delta\psi = \pi$. If $\Delta\psi \neq \pi$, then the steady-state limit cycle frequency ω_1 is determined implicitly by Eq. (42), since $\Delta\psi$ is a function of ω_1. For most cases of practical interest, ω_1 is within a few percent of ω; however, the corresponding percentage error in $\cos\Delta\psi$ may be several times greater. Therefore, for best prediction accuracy, the frequency ω_1 should be used rather than the natural bending frequency ω.

Growth Rate of Transient Bending Oscillations

Let us now restrict Eq. (26) to a transient build-up case in which nozzle #2 is not firing, but in which the bending rate amplitude, P, is not a constant. In particular, in Eq. (26) set $N_1 = N = 1$ and $N_2 = 0$. Since only one cycle of oscillation is considered, $\dot{y}_{cm}$ is the same as $\dot{y}_{cm}$ and $\dot{\theta}_{avg} = \dot{\theta}_{avg}$; hence, these terms disappear. After carrying out the integrations, simplifying, and dividing by the pull-in rate, A, Eq. (26) for this transient build-up case becomes

$$\frac{\omega_1}{\omega}\frac{1}{2\pi\zeta}\frac{\Delta P}{A} = -Q\left(\sin\frac{F_1}{2}\right)\cos\Delta\psi - \frac{P}{A} \tag{43}$$

Equation (43) defines the bending rate amplitude increase per cycle, ΔP, as a function of the structural damping, the rate amplitude, the pull-in rate, the slowly varying portion of the error signal, the nondimensional torque parameter Q, and the characteristics of the rate gyro, filter, and solenoid valve.

Prevention of Buildup to Double-Firing Limit Cycles

By substituting the definition of F_1 from Eq. (19) into Eq. (43) and rearranging it becomes:

$$\frac{E_{avg}}{A} = 1 \pm \frac{P'}{A}\left(1 - \left(\frac{1}{Q\cos\Delta\psi}\right)^2\left[\frac{\omega_1}{\omega}\frac{1}{2\pi\zeta}\frac{\Delta P}{A} + \frac{P}{A}\right]^2\right)^{1/2} \tag{44}$$

Using Eq. (44) in conjunction with Eq. (15), Fig. 6 was computed for the same parameters as were used to compute Fig. 5 except that Q in Fig. 6 is 7.09. Also $\zeta = 0.01$ and $\omega = 123.65$ rad/sec. Figure 6 shows contours of constant $\Delta P/A$. In addition, Fig. 6 shows several boundaries.

The lowest boundaries define the region where, at a given E_{avg}, the filtered bending amplitude P', is too small to reach the upper pull-in line. Due to the restrictions of relation (21), however, nozzle #1 will not actually fire regularly each cycle at a given E_{avg} unless P' is such that the time elapsed between ON and OFF commands, or between OFF and ON commands, is just greater than the nondimensional nozzle time delay, $\omega_1 t_1$. These two boundaries are determined, therefore, by equating $\omega_1 t_1$ to either the function F_1 given by Eq. (19), or to $(2\pi - F_1)$. Thus, after rearrangement, we obtain the following equations defining the boundaries marked, "P' too small for regular cyclic firing."

$$\frac{P'}{A} = \pm\frac{1}{\cos(\omega_1 t_1/2)}\left[1 - \frac{E_{avg}}{A}\right] \tag{45}$$

In the two triangular regions between the line where P' is too small to reach the pull-in rate and the line where P' is too small for regular cyclic firing, the system will operate in an irregular firing mode in which the nozzle fires on some cycles but not on others. In these regions quasi-steady-state, single-sided firing limit cycles of the type discussed above may occur at either large or small disturbance torques, provided the $\Delta P = 0$ contour is reached before crossing the real double-firing boundary (see below). The true rate of amplitude growth in these regions is somewhat less than it would be for the regular cyclic firing assumed by Eq. (44).

The boundary marked "Potential Double-Firing Boundary" in Fig. 6 defines the magnitude of P' which will just reach the lower pull-in line. If the solenoid time delay were zero, double-firing would begin if P' reached this line. For nonzero solenoid time delay, however, according to relation (21), the angle F_2 must exceed the solenoid time delay before nozzle #2 will fire. To determine this boundary, the function

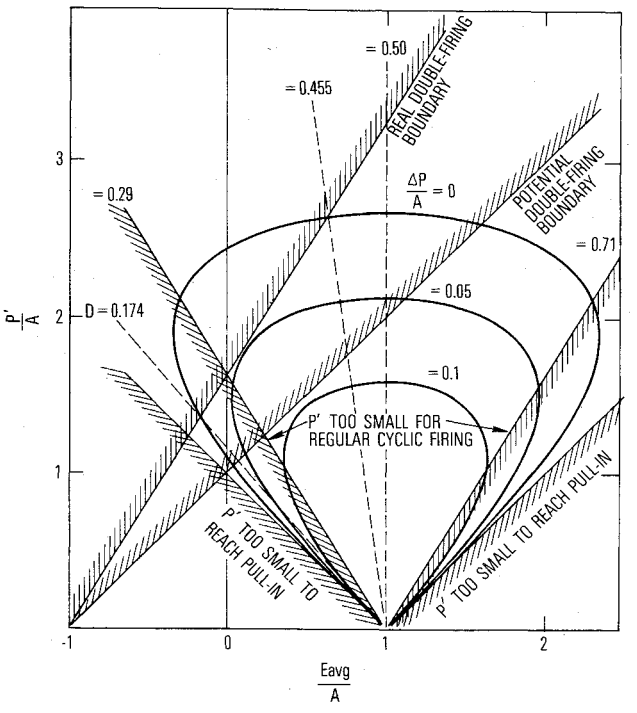

Fig. 6 Bending oscillation growth.

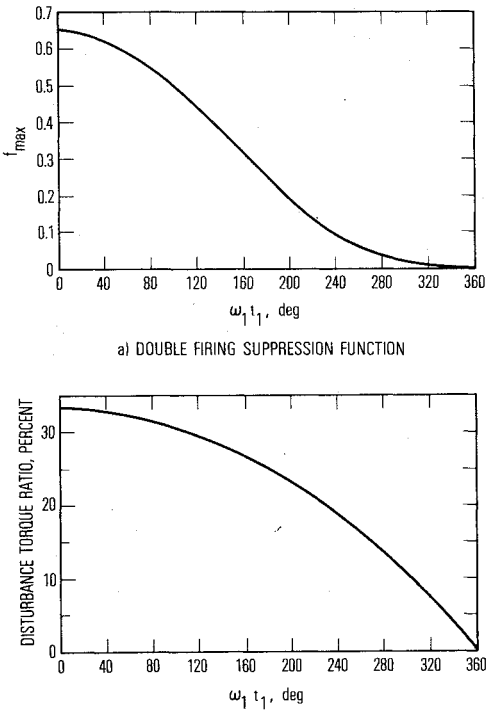

Fig. 7 Double-firing boundary functions.

F_2, Eq. (19) is equated to $\omega_1 t_1$. After rearrangement this gives

$$\frac{P'}{A} = \frac{1}{\cos(\omega_1 t_1/2)}\left[1+\frac{E_{avg}}{A}\right] \tag{46}$$

Equation (46) is shown in Fig. 6 as the "Real Double-Firing Boundary."

Now transient bending oscillations must be excited just in the neighborhood of $E_{avg}=A$, since the nozzle either suddenly applies or removes thrust just at the switching line. Since Fig. 6 shows that the growth rates are greatest in the neighborhood of $E_{avg}=A$, it appears that the transient bending oscillation must grow, at least temporarily. If it grows enough to cross the "Real Double-Firing Boundary," then double-firing limit cycles will result.

Shown also on Fig. 6 are several loci defining steady-state limit cycle operating conditions. These loci are determined by setting $n_1=1$ in Eq. (36), substituting the definition of F_1 from Eq. (19), and rearranging. The result is

$$\frac{P'}{A} = \left[\frac{1-(E_{avg}/A)}{\cos\pi D}\right]; \text{ where } D \equiv \frac{T_D L_D}{T_n L} = \frac{\text{disturbance}}{\text{torque ratio}} \tag{47}$$

For given D, Eq. (47) defines a P'/A vs E_{avg}/A locus of possible steady-state operating conditions. On Fig. 6, these loci are shown for $D=0.174, 0.29, 0.455, 0.5, 0.71$.

During transient conditions in the presence of a constant disturbance torque, the system response will not necessarily operate along a steady-state locus as shown in Fig. 6. When approaching a steady-state condition, however, the tendency of the system will be to approach that condition along the appropriate disturbance torque locus. The system may avoid double-firing if the acting disturbance torque drives the system to a point on its steady-state locus at which $\Delta P=0$ and which is still to the right of the real double-firing boundary. Thus, in the example shown in Fig. 6, the system will avoid double-firing, except possibly for a few firings of nozzle #2, at disturbance torque ratios greater than 0.455. Also, in the example of Fig. 6, it appears that the system will avoid double-firing if D is less than 0.174. For this example, digital simulation results verify this prediction; however, if the Q of the system is larger so that the $\Delta P=0$ contour extends further into the double-firing region, and the growth rate near the boundary is larger, then the system may cross the double-firing boundary in a few cycles even at zero disturbance torque.

Since double-firing bending limit cycles rapidly consume control gas only to maintain a large bending amplitude, it is necessary to design the control system so that double-firing limit cycles cannot occur. Study of Fig. 6 in the light of the above discussion indicates that double-firing limit cycles may be expected to occur at some disturbance torque unless the system is designed to ensure that the $\Delta P=0$ contour never crosses the real double-firing boundary. The required relationship between system parameters to ensure shrinkage of the $\Delta P=0$ contour to just within the double-firing boundary is determined below.

By setting $\Delta P=0$ in Eq. (43), we define the zero growth rate contour. Equation (46) defines the double-firing boundary. By substituting $P=P'/G$ in Eq. (43) with $\Delta P=0$, and subsequent elimination of P'/A between Eqs. (43) and (46), we obtain after rearrangement

$$Q = -\frac{1/G}{(\cos\Delta\psi) f(\cos(\omega_1 t_1/2), E_{avg}/A)} \tag{48}$$

in which we have defined

$$f = \frac{\sin B \cos B}{1-(E_{avg}/A)}; \quad \sin B = \frac{\cos(\omega_1 t_1/2)\,[1-(E_{avg}/A)]}{1+(E_{avg}/A)} \tag{49}$$

The characteristics of the function f are that a given value of f can be obtained from either of two values of (E_{avg}/A). These two values of (E_{avg}/A) correspond to the two possible intersections of the $\Delta P=0$ contour with the real double-firing boundary. At the maximum value of f, however, only one value of E_{avg}/A is possible. This maximum value of f therefore corresponds to making the $\Delta P=0$ contour just touch the real double-firing boundary at a point of tangency. Thus, in order to ensure that the $\Delta P=0$ contour remains within the single-firing region, we must prescribe the

maximum value of the function f in Eq. (48). It can be shown by equating $df/d(E_{avg}/A)$ to zero, that the maximum value of f occurs at a value of the parameter $B=B_1$, where B_1 is determined by

$$\sin B_1 = -\frac{1}{4}\cos(\omega_1 t_1/2) + ([\,\tfrac{1}{4}\cos(\omega_1 t_1/2)\,]^2 + \tfrac{1}{2})^{1/2} \quad (50)$$

The maximum value of f and the corresponding value of E_{avg}/A are given by

$$f_{max} = \cos^3 B_1/2\sin B_1; \quad (E_{avg}/A) = 1 - 2\tan^2 B_1 \quad (51)$$

In summary, the relation between control system parameters which must exist for the $\Delta P=0$ contour to be tangent to the real double-firing boundary is

$$Q = -\frac{1/G}{f_{max}\cos\Delta\psi} \quad (52)$$

Table 2 Values of simulation parameters used

Rate gyro		Vehicle/structure	
ω_{ng}	=undamped frequency =132 rad/sec	M_G	=generalized mass=969.7 kg
ζ_g	=damping factor=0.5	ω	=bending natural frequency =123.65 rad/sec
Filter			
t_2	=time constant=0.01 sec	ζ	=structural damping factor=0.01
Switch		b	=thruster deflection influence coefficient=−0.710
A	=rate deadband=0.2 deg/sec	a	=rate gyro slope influence coef.=-1.388m^{-1} (and as noted below)
Integrator			
$1/\lambda$	=attitude gain=1/1.5 sec^{-1}	c	=disturbance deflection influence coef.=+0.377
Solenoid/Thruster			
t_1	=0.015 sec and 0.005 sec		
T_n	=thruster force=187.5 Newtons	I	=moment of inertia =2831 kg-m^2
L	=distance to vehicle c.g. =1.29m	L_D	=distance to disturbance force station=2.03 m

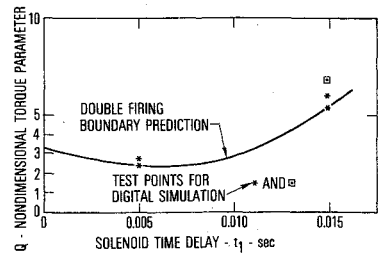

Fig. 8 Double-firing boundary verification by simulation.

Equation (52) is utilized by computing the value of the right side using the applicable values of G, $\Delta\psi$ and f_{max}. Then if Q, the nondimensional torque parameter for the system, is greater than the computed value of the right side of Eq. (52), the system will double-fire. If Q is less than the right side, the system cannot double-fire. Alternatively, for given Q, Eq. (52) determines implicitly the value of the nondimensional filter time constant, $\omega_1 t_2$, required to suppress double-firing. For accurate location of the double-firing boundary, the frequency used in Eq. (52) should be the steady-state frequency, ω_1 determined from Eq. (42).

Disturbance Torque which Maximizes Double-Firing Probability

Knowledge of the disturbance torque which maximizes the probability of double-firing is useful because such knowledge can significantly reduce the number of digital or analog simulation runs needed to complete a verification of the control system. If the $\Delta P=0$ contour extends far beyond the double-firing boundary, then the system will have no difficulty in wandering across the double-firing boundary over a relatively wide range of disturbance torques. However, if the system's $\Delta P=0$ contour is fairly close to tangency with the double-firing boundary, then the band of disturbance torques which will cause double-firing is relatively narrow. The approximate center of this narrow band may be determined analytically by assuming that the system's $\Delta P=0$ contour has shrunk to tangency with the double-firing boundary, and by determining the value of disturbance torque which will cause the steady-state P'/A vs E_{avg}/A locus to pass through the point of tangency.

The point of tangency lies on the real double-firing boundary defined by Eq. (46). The steady-state P'/A vs E_{avg}/A locus is defined by Eq. (47). At the point of in-

Table 3 Comparison of analytic predictions and simulation results

Disturbance torque ratio	Type of limit cycle	Percent difference $=\left[\frac{\text{analytic prediction}}{\text{simulation result}} - 1\right]\times 100$			
		P/A	n_1	n_2	$\theta_{avg}/\lambda A$
0	steady-state, double-firing	+3.5	0	0	0
0.3	steady-state, double-firing	+3.9	0	0	+4.7
0.4	quasi-steady-state, double-firing	+4.3	0	+7.6	+7.1
0.5	quasi-steady-state, double-firing	+5.3	0	+2.2	+5.0
0.6	steady-state, single sided	+3.4	0	0	+3.2
0.7	Steady-state, single-sided	+3.8	0	0	+2.9
0.8	quasi-steady-state, single-sided	+3.0	+5.8	0	+3.3
0.95	quasi-steady-state, single-sided	−14.2	+5.5	0	−8.3

Table 4 Values of a and Q

	$a(m^{-1})$	Q	Boundary value of Q from Eq. (52)
$t_1 = 0.005$ sec	−0.269	2.72	
($\omega_1 t_1 = 35.46$ deg)	−0.243	2.45	2.43
$t_1 = 0.015$ sec	−0.591	5.96	
($\omega_1 t_1 = 104.68$ deg)	−0.545	5.50	5.45

tersection, the values P'/A, as given by both expressions, must be identical; also the parameter B must have the value B_1 in order that the tangency point of the $\Delta P = 0$ contour coincide with the point of intersection; hence, the value of D, which maximizes the probability of double-firing, is defined by:

$$\cos(\pi D) = \left(\frac{1-(E_{avg}/A)}{1+(E_{avg}/A)}\right)\cos(\omega_1 t_1/2) = \sin B_1 \qquad (53)$$

Using Eqs. (50), (51), and (53), the curves of Fig. 7 were computed. Figure 7 shows how f_{max} and D, as given by Eq. (53), vary with $\omega_1 t_1$.

Comparison with Simulation Results

Figure 1 is a block diagram of the essential features of the digital simulation which was used to provide results to compare with the analytic predictions. The simulation was developed for analysis of an actual spacecraft using this type of control system. The values of the simulation parameters which were used are listed in Table 2.

The following parameters which appear in the analytic prediction formulas were calculated from Table 2 data for $t_1 = 0.015$ sec: $Q = (T_n ab/\pi\zeta\omega M_G A) = 14$; $\omega_1 = 121.8$ rad/sec; $\omega_1 t_1 = 104.68°$; $\tan^{-1}\omega_1 t_2 = 50.61°$; $\phi = 80.85°$; $\Delta\psi = 236.14°$; $\cos\Delta\psi = -.557$; and $G = 0.679$.

These values were used to compute the analytic predictions shown in Fig. 5 and used to prepare Table 3. With all the above values held constant, eight simulation runs were made for eight values of the disturbance force ranging from zero up to a value which gave a disturbance torque equal to 95% of the control torque. Each run was ten seconds long, so that a close approximation to the final steady state was obtained. The frequency of the oscillations as determined from the digital print-outs was 121.7 rad/sec. Amplitudes, firing ratios, and average attitude angles were determined also from the digital print-outs. Results are presented in Table 3 in the form of percent differences between the analytic predictions and the simulation results. For convenience, the digital simulation results are spotted on Fig. 5, as well.

Another set of digital simulation runs was made to verify the boundary prediction of Eq. (52). The magnitude of the bending slope at the rate gyro, a, was set to obtain values of Q approximately on, and a little above, the boundary prediction for two values of solenoid time delay, $t_1 = 0.005$ and 0.015 sec. Two values of t_1 were used to test the validity of the f_{max} function in Eq. (52). The values of a and the corresponding Q are listed in Table 4. These four points are shown as asterisks in Fig. 8. The simulation was run with each of the above four values of a and with a disturbance torque of 32%.

Analysis of the four simulation runs gave the following results. The attitude control system did not double-fire at $Q = 2.45$, $t_1 = 0.005$ sec, or at $Q = 5.50$, $t_1 = 0.015$ sec. The system did double-fire for the two cases where the Q value was above the boundary curve by 9 to 12%.

Apparently, the approximations of the analysis result in a slightly conservative boundary prediction, since the simulation cases which were essentially on the boundary did not double-fire. The simulation results clearly demonstrate the validity of the boundary prediction to within about 10% of the value of Q. No attempt was made to verify the prediction to a smaller percentage difference, although additional simulation runs at intermediate values of Q might provide this verification.

It is possible not to achieve double-firing even though the operating parameters potentially permit double-firing if the disturbance torque ratio is not close to the value indictated in Fig. 7b. To verify this possibility, a simulation was made with conditions identical to those of Fig. 6 ($t_1 = 0.015$; $Q = 7.09$), but with a disturbance torque of 15% rather than 32%. This case is indicated as the squared point in Fig. 8. This case does double-fire at 32% disturbance. The system would not double-fire at 15% disturbance.

References

[1] LaSalle, J.P. and Lefschetz, S. *Stability of Liapunov's Direct Method with Applications,* Ch. 1, Academic Press, N.Y., 1961.

[2] Minorsky, N., *Theory of Nonlinear Control Systems,* Chs. 4-5, McGraw-Hill, N.Y., 1969.

[3] Dragoslav, D.D., *Nonlinear Systems—The Parameter Analysis and Design,* Chs. 3-8, Wiley, N.Y., 1969.

[4] Weissenberger, S., "Stability-Boundary Approximations For Relay-Control Systems Via A Steepest-Ascent Construction of Lyapunov Functions," *Transactions of the ASME, Journal of Basic Engineering,* Ser. D, Vol. 88, June 1966, pp. 419-428.

[5] Kalman, R.E. and Bertram, J.E., "Control System Design Via the Second Method of Liapunov," *Transactions of the ASME, Journal of Basic Engineering,* Vol. 82, 1960, pp. 371-400.

[6] Brockett, R.W., "The Status of Stability Theory for Deterministic Systems," *IEEE Transactions on Automatic Control,* Vol. AC-11, July 1966, pp. 596-606.

[7] Gervarter, W.B., "Basic Relations for Control of Flexible Vehicles," *AIAA Journal,* Vol. 8, April 1970, pp. 666-672.

[8] Meirovitch, L. and Calico, R.A., "A Comparative Study of Stability Methods for Flexible Satellites," *AIAA Journal,* Vol. 11, Jan. 1973, pp. 91-98.

[9] Thomson, W.T. and Reiter, G.S., "Attitude Drift of Space Vehicles," *Journal of the Astronautical Sciences,* Vol. III, Summer 1960, pp. 29-34.

[10] Meirivitch, L., "Attitude Stability of an Elastic Body of Revolution in Space," *Journal of the Astronautical Sciences,* Vol. VIII, Winter 1961, pp. 110-113.

[11] Truxal, J.G., *Automatic Feedback Control System Synthesis,* McGraw-Hill, 1955, Ch. 10.

[12] Loesch, F. and Hecht, C., "Work/Energy Principles Applied to a Deadband Attitude Control System to Analyze Bending Limit Cycles," Aerospace Corp., Report prepared for Space and Missile System Organization, Air Force Systems Command, Los Angeles, Cal., SAMSO-TR-75-121, March 21, 1975.